Article

Titanium:sapphire-on-insulator integrated lasers and amplifiers

https://doi.org/10.1038/s41586-024-07457-2

Received: 5 October 2023

Accepted: 23 April 2024

Published online: 26 June 2024

Check for updates

Joshua Yang[1,3], Kasper Van Gasse[1,2,3], Daniil M. Lukin[1,3], Melissa A. Guidry[1], Geun Ho Ahn[1], Alexander D. White[1] & Jelena Vučković[1]✉

Titanium:sapphire (Ti:sapphire) lasers have been essential for advancing fundamental research and technological applications, including the development of the optical frequency comb[1], two-photon microscopy[2] and experimental quantum optics[3,4]. Ti:sapphire lasers are unmatched in bandwidth and tuning range, yet their use is restricted because of their large size, cost and need for high optical pump powers[5]. Here we demonstrate a monocrystalline titanium:sapphire-on-insulator (Ti:SaOI) photonics platform that enables dramatic miniaturization, cost reduction and scalability of Ti:sapphire technology. First, through the fabrication of low-loss whispering-gallery-mode resonators, we realize a Ti:sapphire laser operating with an ultralow, sub-milliwatt lasing threshold. Then, through orders-of-magnitude improvement in mode confinement in Ti:SaOI waveguides, we realize an integrated solid-state (that is, non-semiconductor) optical amplifier operating below 1 μm. We demonstrate unprecedented distortion-free amplification of picosecond pulses to peak powers reaching 1.0 kW. Finally, we demonstrate a tunable integrated Ti:sapphire laser, which can be pumped with low-cost, miniature, off-the-shelf green laser diodes. This opens the doors to new modalities of Ti:sapphire lasers, such as massively scalable Ti:sapphire laser-array systems for several applications. As a proof-of-concept demonstration, we use a Ti:SaOI laser array as the sole optical control for a cavity quantum electrodynamics experiment with artificial atoms in silicon carbide[6]. This work is a key step towards the democratization of Ti:sapphire technology through a three-orders-of-magnitude reduction in cost and footprint and introduces solid-state broadband amplification of sub-micron wavelength light.

Titanium:sapphire (Ti:sapphire) laser systems[5,7] play an essential part in both fundamental research and technological applications, including the demonstration of the first optical frequency comb[1], generation of optical pulses as short as two oscillations of the electrical field[8], two-photon microscopy and optogenetics[2,9,10] and demonstrations of on-chip laser-driven particle accelerators[11,12]. As a solid-state (that is, non-semiconductor) gain medium, Ti:sapphire has exceptional properties, possessing the widest gain bandwidth of any laser crystal (190 THz, wavelength range 650–1,100 nm), a large emission cross-section and a four-level structure[5]. Consequently, mode-locked and continuous-wave Ti:sapphire lasers are unmatched in performance and are essential in disciplines such as quantum optics and atomic physics[3,4,13,14]. However, the excellent performance of Ti:sapphire lasers comes at a cost: commercial systems are bulky, expensive and require high-power pump lasers, prohibiting their widespread use in many real-world applications that demand compactness and scalability.

Photonic integrated circuit technologies are revolutionizing laser systems by delivering compactness, scalability and cost efficiency that are impossible to achieve in table-top systems, leveraging wafer-scale fabrication abilities in material platforms such as silicon-on-insulator[15], thin-film lithium niobate[16] and silicon nitride[17]. By integrating passive photonics elements with III–V semiconductor optical amplifiers, on-chip laser systems have already been realized in wavelength ranges optimized for telecommunications[18–20] and are now moving towards the near-infrared (NIR) and visible ranges[21–23]. However, integrated semiconductor laser and amplifier systems face several limitations, most notably limited gain bandwidth and poor high-power handling abilities because of two-photon[24] and free-carrier absorption in high-confinement waveguides, limiting on-chip pulse energies to several picojoules[25]. An emerging alternative to on-chip III–V systems is integrated solid-state gain media based on rare-earth ions. Recently, by implanting ultralow-loss silicon-nitride waveguides with erbium ions, high-performance solid-state waveguide amplifiers and lasers have been demonstrated[26,27] exceeding 100 pJ pulse energies; however, these efforts, along with those in other rare-earth systems, are limited to wavelengths longer than 1 μm. Thus, the aforementioned applications that require high-performance abilities of Ti:sapphire lasers have not been able to benefit from photonic circuit integration. An integrated solid-state laser and amplifier operating both in the visible and in the NIR wavelength ranges would have a substantial impact in the areas of

[1]E. L. Ginzton Laboratory, Stanford University, Stanford, CA, USA. [2]Photonics Research Group, Ghent University-imec, Ghent, Belgium. [3]These authors contributed equally: Joshua Yang, Kasper Van Gasse, Daniil M. Lukin. ✉e-mail: jela@stanford.edu

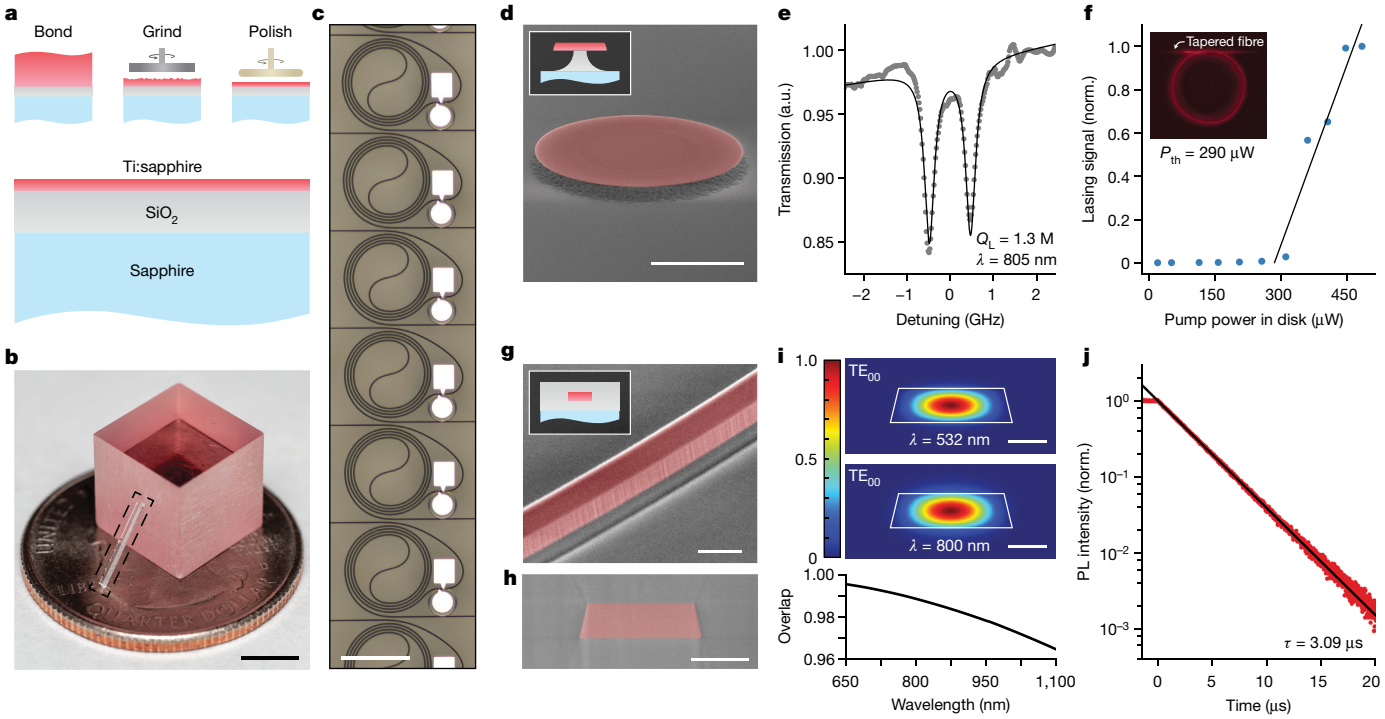

Fig. 1 | Low-loss photonics and sub-milliwatt threshold Ti:sapphire laser in monocrystalline sapphire-on-insulator. a, Process flow of Ti:SaOI preparation. **b**, Photograph of an array of on-chip Ti:SaOI lasers (inside dashed rectangle) resting on a Ti:sapphire bulk crystal. **c**, A close-up optical micrograph of fabricated devices. **d**, SEM image of a photolithographically patterned Ti:SaOI microdisk resonator (Ti:sapphire layer is false coloured). Inset, microdisk geometry and material stack. **e**, Quality factor of 1.3×10^6 measured in transmission at 805 nm, fit to a split Lorentzian. **f**, Lasing signal of the microdisk resonator (measured using spectrometer) with increasing pump power in the resonator, showing lasing threshold pump power of 290 μW. Inset, optical microscope image of the resonator under excitation (with 532 nm light filtered), showing spontaneous emission collected vertically. **g**, SEM image of a Ti:SaOI waveguide fabricated with electron-beam lithography. Inset, waveguide geometry and material stack. **h**, SEM of waveguide cross-section. **i**, Simulated mode intensity profile at the pump (532 nm; top) and lasing (800 nm; middle) wavelength, with modal intensity overlap $\Gamma_{p,s}$ of 98.8%. Calculated intensity overlap (bottom) between the pump mode (532 nm) and signal mode in the range 650–1,100 nm. **j**, Exponential decay of waveguide fluorescence with an optical lifetime of 3.09 μs. a.u., arbitrary units; norm., normalized; PL, photoluminescence; TE_{00}, fundamental TE mode. Scale bars, 5 mm (**b**); 200 μm (**c**); 20 μm (**d**); 1 μm (**g**); 750 nm (**h**); and 500 nm (**i**).

science and technology in which cost, size and scalability considerations are important.

Accordingly, efforts towards miniaturization of Ti:sapphire lasers have a long history. Limitations in scalability for current Ti:sapphire laser systems have been primarily because of the short fluorescence lifetime of the Ti^{3+} ion, which, when combined with the large disparity between pump (490–532 nm) and lasing (650–1,100 nm) wavelengths, increases system complexity and necessitates very high pump intensities before achieving appreciable amplification and lasing. To address this issue, approaches such as pulsed laser deposition of waveguides[28], laser written waveguides[29,30], optical fibres[31,32] and machined whispering-gallery-mode lasers[33] have been used to reduce mode volume and lower the lasing threshold. A recent demonstration of bonding Ti:sapphire to a silicon-nitride photonic chip to achieve lasing by evanescent coupling represents one of the first nanophotonic Ti:sapphire lasers[34], but this approach poses challenges for achieving substantial gain due to limited modal overlap. As a result, a practical on-chip Ti:sapphire laser system has not yet been realized. The highest single-mode output power in an on-chip Ti:sapphire laser is only 40 nW (ref. 34), and a tunable laser has yet to be demonstrated. Furthermore, no attempt to realize an integrated Ti:sapphire amplifier has been reported, to our knowledge.

In this work, we address these challenges and demonstrate chip-integrated Ti:sapphire lasers and waveguide amplifiers that deliver the power, stability and tunability relevant for practical applications in research and technology. Our approach is based on an architecture that attains the fundamental limit of photonic mode confinement and overlap, using a low-loss, thin-film monocrystalline sapphire-on-insulator photonics platform, enabling a lasing threshold power of 290 μW. We demonstrate an integrated Ti:sapphire broadband waveguide amplifier, enabling unprecedented on-chip operation at a peak output power of 1 kW without pulse distortion. We then realize the tunable integrated Ti:sapphire laser, now occupying a footprint of less than 0.15 mm^2, with one of the widest tuning ranges for any fully integrated laser[22,35,36], and, in a proof-of-concept application, use a Ti:sapphire laser array for a quantum optics experiment with artificial atoms in silicon carbide[6].

Ti:SaOI photonics platform

The Ti:SaOI fabrication process is shown in Fig. 1a. The damage-free monocrystalline Ti:sapphire platform is produced by grinding and polishing (Methods), following the approach demonstrated for wafer-scale production of other high-quality monocrystalline photonics platforms, such as silicon-carbide-on-insulator[37]. Figure 1b shows a photograph of a completed Ti:SaOI microchip (8 × 0.5 mm) resting on a cube of bulk Ti:sapphire crystal. The magnified view of the chip is presented in Fig. 1c, showing an array of Ti:SaOI lasers (see section 'Tunable Ti:sapphire laser on chip').

To assess the intrinsic photonic qualities of the Ti:SaOI platform, we fabricate whispering-gallery-mode resonators using a photoresist pattern-transfer process that results in an ultralow-roughness surface (Methods). Owing to the four-level structure of the Ti^{3+} gain medium, the lasing transition of Ti^{3+} in the absence of pumping has no impact on

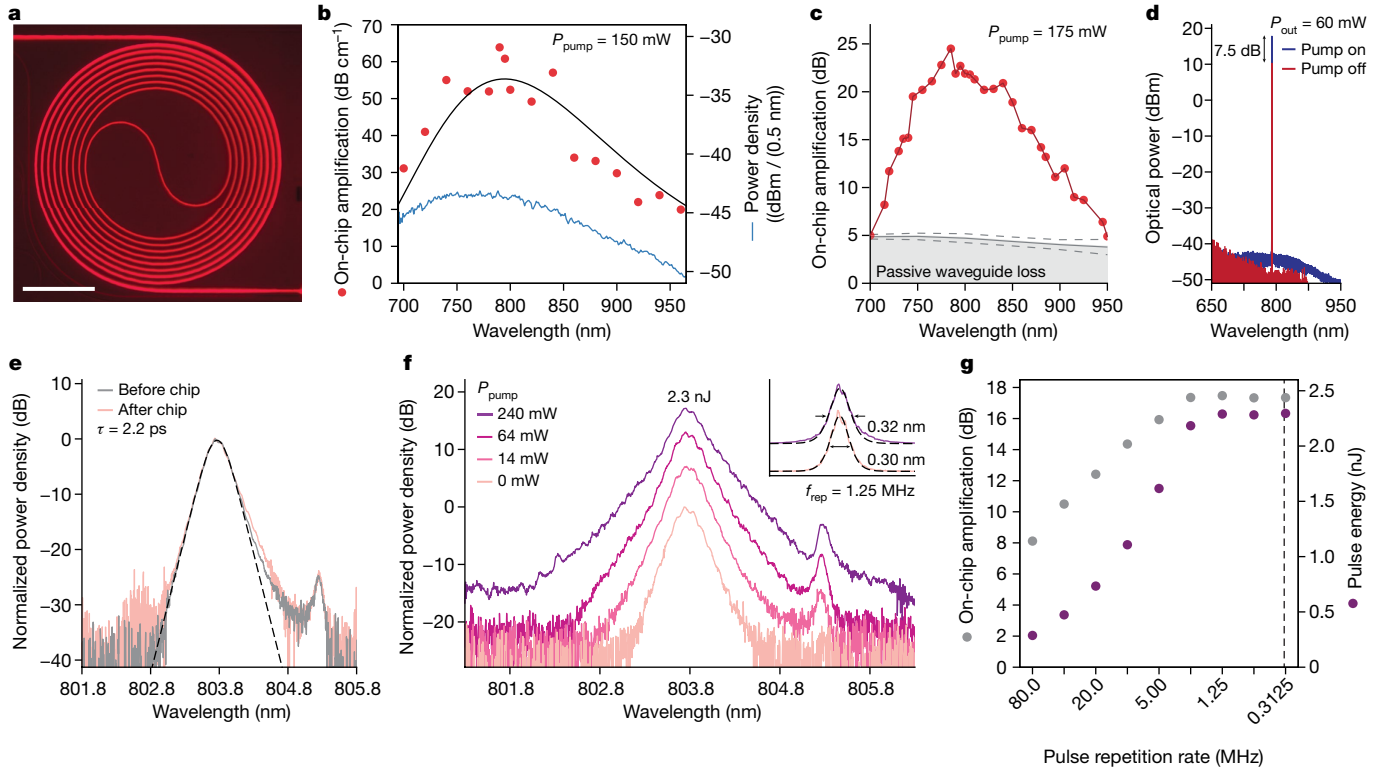

Fig. 2 | Integrated optical amplifier in Ti:SaOI. a, Optical image of an 8-mm waveguide amplifier pumped from both ends (532 nm pump filtered). **b**, ASE spectrum collected from a 0.5-mm waveguide when no input signal is present (blue). Measured small-signal gain (dB cm^{-1}) for the same waveguide (red). The fit to the calculated gain profile is shown in black[60]. **c**, Measured small-signal gain for an 8-mm long amplifier (red), with a pump power of 175 mW and measured passive waveguide losses (grey). Standard error is shown by dashed lines. **d**, Spectrum of the amplified continuous-wave output signal at peak recorded output power of 60 mW. **e**, Normalized spectra of a picosecond pulse before and after propagation in the amplifier, showing no nonlinear distortion. **f**, Spectrum of the amplified pulses (at a repetition rate of 1.25 MHz) for varying magnitude of amplification. Inset, unamplified and maximally amplified output on a linear scale, showing that the pulse remains transform-limited with minor distortion of the tails. **g**, The dependence of amplification and output pulse energy on the repetition rate. Vertical dashed line indicates the lifetime of the gain medium ($1/\tau$). Scale bar, 100 µm (**a**).

the absorption in the emission band, permitting direct characterization of passive losses. Addressing the whispering-gallery-mode resonator with a tunable laser using a tapered fibre, we observe the intrinsic quality (Q) factors up to 1.3 million at a wavelength of 805 nm (Fig. 1e) in 50-µm diameter resonators, corresponding to a propagation loss of 0.5 dB cm^{-1}. By thermally tuning the microdisk, it is brought in resonance with the 532-nm pump laser. We observe single-mode lasing with a threshold pump power of 290 µW (Fig. 1f), a reduction by a factor of 22 from previous demonstrations[33,34]. This is a consequence of the tight modal confinement, maximal modal overlap with high-quality gain material and low-loss fabrication.

Direct pattern transfer from photoresist to Ti:sapphire limits the resolution and sidewall angle of structures, precluding the realization of many integrated photonics functionalities. To this end, we develop a pattern-transfer process based on a secondary hard mask layer consisting of 200 nm of chromium (deposited by electron-beam evaporation). Electron-beam photoresist (FOx-16, Corning) is used to define the pattern in the chromium mask (Methods). This process results in waveguides with a near-vertical (11°) sidewalls and sub-100 nm minimum feature size (Fig. 1g,h). We note that this process is also compatible with deep UV photolithography for high-throughput fabrication[21]. This high-confinement, nearly single-mode waveguide geometry achieves a near-unity broadband overlap of the pump and lasing modes (99.5% at 650 nm and 96.5% at 1,100 nm), a crucial advantage of the Ti:SaOI laser platform that unlocks the ability to reach the ultimate limit of efficiency and low-power operation in Ti:sapphire lasers. Of importance is that the thin film of Ti:sapphire preserves the quality of the bulk gain medium, confirmed by an excited-state lifetime consistent with that of bulk Ti:sapphire[5] (Fig. 1j and Methods). We conclude that the Ti:SaOI platform features excellent metrics for laser fabrication, both in passive optical losses and in the active gain medium.

Ultrawide-band waveguide amplifiers in Ti:SaOI

Amplifiers are essential companions to lasers, allowing for the reversal of losses in coherent signals and enabling the reach of power levels beyond the ability of a laser source. Here, using the Ti:SaOI platform, we demonstrate an integrated solid-state amplifier operating below 1 µm, which possesses marked power handling and bandwidth among both integrated and table-top state-of-the-art systems.

Strong pump confinement (effective mode area 0.62 $µm^2$) and near-unity mode overlap in nanophotonics result in modest power requirements to reach saturation of the gain medium, enabling high gain even at low pump power. The Ti:SaOI waveguide amplifier (Fig. 2a) is fully integrated and ultracompact (footprint <0.20 mm^2). To measure the intrinsic gain characteristics of Ti:sapphire nanophotonics, we first examine a short (length of 485 µm) waveguide, in which the effects of pump absorption, passive losses and spatial mode mixing are negligible. A commercial continuous-wave Ti:sapphire laser (SolsTiS, M Squared) is used as a wavelength-tunable signal. At a pump power of 150 mW, we observe a peak gain of 64 dB cm^{-1}, and more than 30 dB cm^{-1} across a 100-THz bandwidth (Fig. 2b). In the absence of an input signal, the waveguide is also a source of bright amplified spontaneous emission (ASE) with a bandwidth exceeding 100 THz (Fig. 2b), the widest demonstrated so far. This broadband source, which can be readily

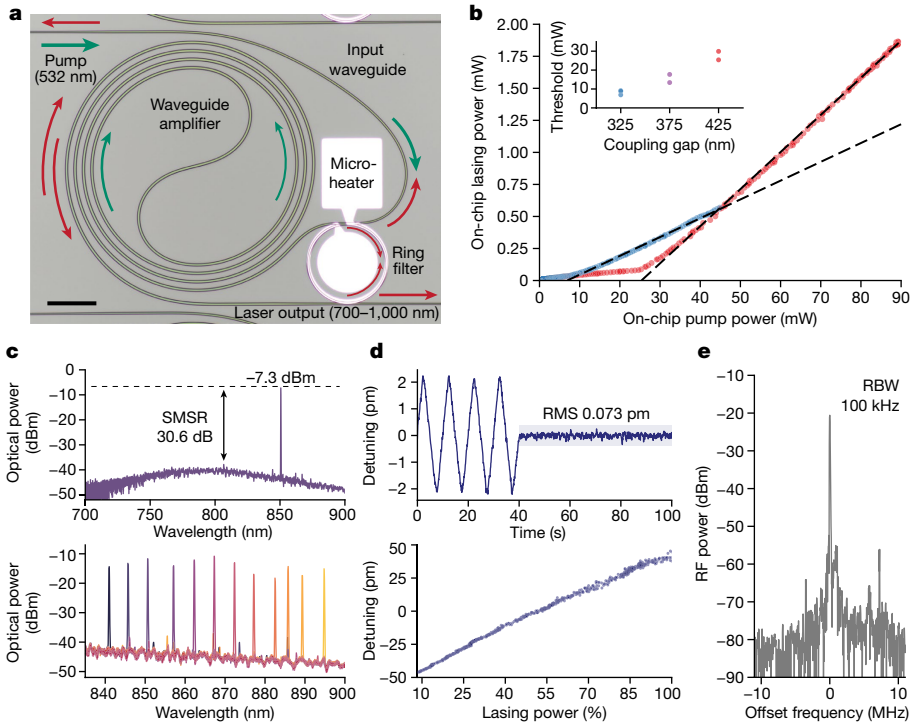

Fig. 3 | Widely tunable, narrow-linewidth chip-integrated Ti:sapphire laser. **a**, Optical image of a laser. **b**, Output power of the Ti:SaOI tunable laser compared with pump power (multimode operation) for the largest (red) and smallest (blue) coupling gap. Inset, dependence of threshold power on microring–waveguide coupling gap across the seven-device laser array. **c**, Lasing spectrum (top) and ASE background (here and onwards, operation is single mode). Coarse wavelength tuning (bottom) by the microheater. **d**, Fine wavelength tuning (top) and stabilization by feedback applied on the microheater. Mode-hop-free tuning (bottom) by 91 pm (36.4 GHz) by modulation of pump power. **e**, Measured laser linewidth of 140 kHz, using heterodyne technique. SMSR, side-mode suppression ratio; RMS, root-mean-square; RBW, resolution bandwidth; RF, radiofrequency. Scale bar, 50 µm (**a**).

coupled to an optical fibre, may find use in medical applications such as optical coherence tomography[38,39].

To measure total achievable amplification, we use a spiral waveguide with a length of 8 mm, in which the pump is nearly fully absorbed, for the rest of the experiments in this section. We note that, owing to the four-level structure of Ti^{3+}, no signal reabsorption takes place in weakly pumped sections of the waveguide, and the material gain is always positive. The small-signal (3 µW input power) amplification of an 8-mm-long Ti:SaOI waveguide is shown in Fig. 2c, reaching a peak on-chip gain of more than 20 dB, with a pump power of 175 mW. Here the maximum gain was limited by parasitic lasing caused by reflections from the waveguide facets, similar to that reported for on-chip erbium amplifiers in ref. 26. Higher gain can be achieved by a reflection-suppressing design or packaging. Figure 2d shows large-signal amplification, with an output continuous-wave power of 60 mW at 790 nm (400 mW pump power).

High-performance mode-locked lasers have long eluded photonic integration because of the challenge of amplifying ultrashort, high-peak-power optical pulses. These lasers are pivotal for advancing diverse fields such as supercontinuum and optical frequency comb generation[1], two-photon microscopy[2] and dual-comb metrology[40]. Here we show that the combination of high gain-per-unit-length, absence of two-photon absorption, weak Kerr nonlinearity ($n_2 = 3 \times 10^{-20}$ m^2 W^{-1}) (ref. 41) and excellent power handling of Ti:SaOI enables unprecedented on-chip distortion-free pulsed amplification. We use a commercial picosecond mode-locked Ti:sapphire laser (Tsunami, Spectra-Physics) as the input signal. To assess the degree of passive nonlinear distortion of a pulse propagating in the amplifier (Supplementary Information), we compare the pulse spectrum before and after passing through the waveguide, without amplification. Negligible spectral distortion is observed for an input pulse energy of 120 pJ (Fig. 2e). The shape of the output pulse for varying pump power is shown in Fig. 2f, which shows minimal change in shape at peak gain of 17 dB, which corresponds to a pulse energy of 2.3 nJ and a peak power of 1.0 kW (240 mW pump power). This is more than an order of magnitude greater than the highest integrated pulsed amplification demonstrated so far, to our knowledge, based on rare-earth waveguides[26,42,43], and is the only integrated high-power transform-limited amplifier for any wavelength. The Ti:SaOI amplifier constitutes the first realization of on-chip pulsed amplification below 1 µm and demonstrates the potential of the platform for the realization of a high-performance integrated mode-locked laser.

Tunable Ti:sapphire laser on chip

Owing to the four-level structure of Ti:sapphire, the demonstrated high-gain waveguide amplifier straightforwardly enables the realization of a tunable, non-resonantly pumped single-mode laser when combined with a spectrally selective re-circulating element. In this section, we demonstrate a versatile Ti:SaOI laser based on this architecture. The laser schematic is presented in Fig. 3a. The re-circulating element is a microring resonator integrated with a platinum microheater for spectral tuning, isolated from the gain section and thus avoiding temperature-induced gain degradation. For lasing to occur at a given wavelength, two conditions must be met: (1) the round-trip accumulated phase must be zero; and (2) the microring must be on resonance with the lasing wavelength (the transmission of the ring resonator must be sufficient for gain to overcome round-trip loss). This interplay of the delay line phase and microring resonance condition enables widely tunable, single-mode operation. Furthermore, this geometry benefits from the disparate pump and signal wavelengths. Despite broadband coupling between the waveguide and microring in the lasing band for the fundamental TE mode, there is negligible coupling at the pump wavelength, and thus the architecture operates

purely non-resonantly and maintains near-unity modal overlap (Fig. 1i). Thus, insensitive to the spectral purity of the pump source, this laser can be pumped with any laser diode in the range of 450–550 nm. Figure 3c shows single-mode operation across greater than 50-nm wavelength range in a single device. The geometry is optimized either for low-threshold pump power (as low as 6.9 mW) or for high efficiency and output power (2.9% and 1.8 mW, respectively, in multimode operation), as shown in Fig. 3b. Multimode lasing in the range of 790–930 nm has been observed among the devices studied in this work. To realize lasing across the full gain bandwidth of Ti^{3+} (650–1,100 nm), an optimized filter–ring coupling geometry is necessary to compensate for the nonuniformity in the gain profile (Fig. 2c).

We investigate the spectral stability and mode-hop-free tunability of the laser using a high-precision wavelength meter (WS7, HighFinesse). By applying feedback to the microheater, we realize triangular tuning across 4 pm and wavelength stabilization to 0.073 pm root-mean-square (RMS) (Fig. 3d). An even greater single-mode, mode-hop-free tuning range is possible using pump power modulation. Figure 3d shows mode-hop-free tuning of 91 pm (36.4 GHz), matching that of commercial Ti:sapphire laser systems. Finally, we measure the instantaneous linewidth of 140 kHz by a heterodyne measurement against a commercial Ti:sapphire laser (Fig. 3e). The laser linewidth can be further reduced by increasing the effective waveguide cavity length and by increasing the quality factor of the microring resonator[22,44], as has been shown with integrated lasers based on semiconductor gain media, or by self-injection locking to an external high-quality-factor silicon-nitride microring resonator[18].

For the results presented so far, we have used a table-top green laser (Verdi, Coherent) as the pump, because of its convenience and large available power. However, these pump lasers are bulky (10 kg excluding power supply) and expensive (US$30,000). Thus, chip integration of the Ti:sapphire laser without miniaturization of the pump does not achieve scalability. Owing to the non-resonant, low-threshold Ti:SaOI laser design presented in this work, the spectral coherence of the pump is irrelevant, allowing us to use an off-the-shelf laser diode (OSRAM, retail price US$37 on www.mouser.com) as a miniature pump. The experimental details and lasing spectra are presented in the Methods and Extended Data Fig. 1, respectively. This complete integrated system driven by a cheap incoherent light source is the decisive first step towards democratizing the Ti:sapphire laser technology for real-world applications.

Using a Ti:SaOI laser for optical control of cavity-integrated artificial atoms

We proceed to demonstrate an application of the presented integrated Ti:sapphire laser array in a practical laboratory setting. We perform a cavity quantum electrodynamics (QED) experiment with solid-state artificial atoms in silicon carbide, with the Ti:SaOI laser array as the sole light source. Colour centres in materials such as silicon carbide and diamond[45] can enable scalable, integrated, optically interfaced spin qubits for advancing quantum sensing[46], quantum networks[47] and many-body physics[48]. Colour centres are typically integrated into nanophotonic resonators to enhance their light–matter interaction, as well as to mediate atom–atom coupling to build entanglement[6,49]. The operation of an atomic system requires multiple lasers with stable and precisely tunable frequencies. Here we replace all table-top lasers sources with a Ti:SaOI laser array.

The experiment is shown in Fig. 4a. The output of two Ti:SaOI lasers on one chip is coupled into a single-mode fibre and routed to the cavity QED system. The cavity consists of a silicon carbide whispering-gallery-mode resonator[50] with a fibre interface[51], situated in a 4.5-K cryostat. The details of the experiment follow closely our previous work performed with table-top commercial lasers in ref. 6. The system can be excited through the waveguide, or by free-space optical access from above, which enables diffraction-limited imaging of the colour centres in the resonator using scanning beams. The artificial atoms used in this work are silicon vacancy (V_{Si}) colour centres. A simplified level structure of the V_{Si} is shown in Fig. 4a. The V_{Si} features two optical transitions, at 861.6 nm and at 858.9 nm, referred to as V1 and V1′, respectively (ref. 52), and is also amenable to above-resonant excitation with wavelengths below 830 nm.

To achieve tunable operation at the precise wavelengths of V1 and V1′ transitions, we operate in the few-mode (two to five modes) lasing regime and filter the desired mode with an optical filter. In the future, more complex Vernier filter design will enable robust purely single-mode operation covering the entire tuning range without gaps. For above-resonant excitation, in which higher power is required but the wavelength does not need to be tuned precisely, we operate in single-mode regime. The experiment begins by tuning the resonator onto the V1 transition. This is done by cryogenic gas deposition while monitoring the waveguide transmission[6]. Figure 4b shows a critically coupled optical mode of the cavity scanned with the Ti:SaOI laser (and a commercial laser for comparison). Once the cavity is on resonance, raster-scanning of the Ti:SaOI laser is done at 823 nm (output power 0.160 mW) from free space to detect the spatial distribution of emitters by waveguide-coupled photoluminescence (Fig. 4c) with photon counting performed with a superconducting nanowire single-photon detector (SNSPD). However, other parasitic optically active defects are excited as well, and not all fluorescence spots correspond to desired artificial atoms. Ultimately, resonant excitation by V1′ optical transition is the optimal means of excitation. To verify whether a fluorescent spot is a silicon-vacancy colour centre, we park the Ti:SaOI laser at one spot and perform resonant absorption spectroscopy by continuous tuning of the laser over 160 pm across the V1′ optical transition and detection of emission into the V1 transition. This measurement is shown in Fig. 4d. Finally, we confirm that the other fluorescence in the above-resonant scan (Fig. 4c) does not correspond to silicon-vacancy colour centres by performing raster-scanning of the laser beam parked at 858.925 nm and observing no other dominant fluorescence spots (Fig. 4e). We have thus identified the spatial location and exact frequency of a colour centre after co-aligning it spectrally with the cavity to achieve Purcell enhancement, using an integrated Ti:sapphire laser array. We note that, in this experiment, the Ti:SaOI laser was used in a plug-and-play configuration, replacing the table-top laser directly without any need for modifications to the experimental setup. The demonstrated Ti:SaOI platform will permit simultaneous control of many emitters at disparate frequencies and play a key part in achieving scalability of both atomic and solid-state quantum systems[53].

Discussion

In this work, we have demonstrated chip-integrated, broadband tunable and scalable Ti:sapphire lasers and amplifiers in a monocrystalline sapphire-on-insulator photonics platform. Already, without design optimization, lasers in this study match or exceed the tuning range of commercial solutions. The low threshold and non-resonantly pumped compact Ti:SaOI lasers replace complex and expensive (>US$100,000) Ti:sapphire laser systems, enabling a reduction of three orders of magnitude in cost and size, as well as a drop of two orders of magnitude in power consumption of the full system. This will result in a democratization of high-performance Ti:sapphire lasers, with a substantial impact on research and technology.

Beyond vastly increasing the accessibility of Ti:sapphire lasers, Ti:SaOI also unlocks new modalities of this traditional laser crystal. Through nanophotonic confinement, the highly efficient generation of ultrabroad ASE shown in this work would serve as a versatile fibre-coupled source for high-resolution optical coherence tomography[38]. Overcoming the limitations of III–V semiconductor amplifiers, the demonstration of a Ti:SaOI waveguide amplifier, with a peak

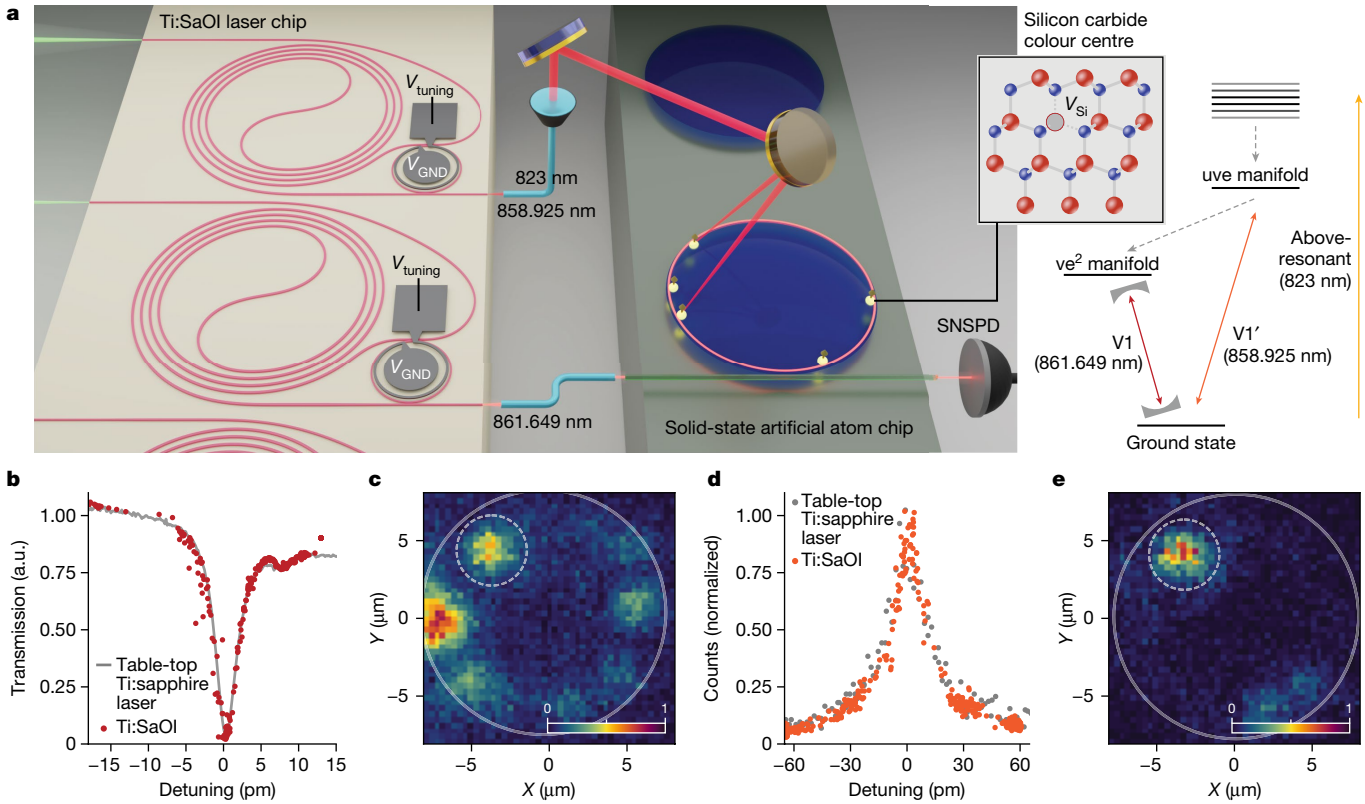

Fig. 4 | Quantum photonics with artificial atoms driven by integrated Ti:SaOI lasers. a, Illustration of the demonstration. A Ti:SaOI laser array is used to control a solid-state cavity QED system in silicon carbide. Lasers control the system by free-space excitation as well as by a waveguide interface. The level structure of the V_{Si} colour centre is shown on the right. **b**–**e** The flow of the cavity QED experiment. **b**, The resonator frequency is tuned until an optical mode overlaps with the V1 transition of the colour centre, as confirmed by the cavity transmission scan. Detuning is relative to 861.649 nm. For comparison, we show the transmission recorded both with a table-top Ti:sapphire laser and with our integrated Ti:SaOI laser. **c**, With the cavity on resonance, an above-resonant raster scan is performed at 823 nm. A fluorescence spot (dashed circle) is identified as a colour centre candidate. **d**, The free-space laser beam is focused on the spot, and resonant absorption spectroscopy is performed by tuning the laser across 120 pm to identify the V1′ transition. Detuning is relative to 858.925 nm. **e**, The raster scan is repeated with the resonant laser at the absorption line peak. The high contrast scan shows that a single colour centre is coupled to the resonator, whereas the other features in **c** are parasitic fluorescence. uve and ve^2 represent the electron orbitals[61] a.u., arbitrary units; GND, ground.

gain of 64 dB cm^{-1} and operating at 1.0 kW peak output power, opens the doors to unprecedented high-power, distortion-free amplification of both continuous-wave and pulsed light within the ultrawide bandwidth of 650–1,100 nm. This work addresses one of the main challenges in the development of on-chip mode-locked lasers and self-referenced optical frequency combs in a sought-after wavelength range previously out of reach[54,55]. Beyond laser technologies, the monocrystalline sapphire-on-insulator platform shown in this work may find uses in demanding applications in the blue and ultraviolet range, owing to its ultrawide bandgap of 10 eV and pristine crystal quality[56].

The integration of Ti:sapphire technology on chip is a decisive step towards massively scalable Ti:sapphire systems, both monolithic and integrated with passive materials. The approach presented in this work is compatible with co-integration in platforms such as silicon nitride and lithium niobate to realize sub-micron-wavelength frequency-agile Ti:sapphire lasers, integrated frequency-doubled lasers[57], on-chip supercontinuum generation[58] and integrated optical parametric amplifiers[59].

Online content

Any methods, additional references, Nature Portfolio reporting summaries, source data, extended data, supplementary information, acknowledgements, peer review information; details of author contributions and competing interests; and statements of data and code availability are available at https://doi.org/10.1038/s41586-024-07457-2.

1. Holzwarth, R. et al. Optical frequency synthesizer for precision spectroscopy. *Phys. Rev. Lett.* **85**, 2264–2267 (2000).
2. Helmchen, F. & Denk, W. Deep tissue two-photon microscopy. *Nat. Methods* **2**, 932–940 (2005).
3. Semeghini, G. et al. Probing topological spin liquids on a programmable quantum simulator. *Science* **374**, 1242–1247 (2021).
4. Ebadi, S. et al. Quantum phases of matter on a 256-atom programmable quantum simulator. *Nature* **595**, 227–232 (2021).
5. Moulton, P. F. Spectroscopic and laser characteristics of Ti:Al_2O_3. *J. Opt. Soc. Am. B* **3**, 125–133 (1986).
6. Lukin, D. M. et al. Two-emitter multimode cavity quantum electrodynamics in thin-film silicon carbide photonics. *Phys. Rev. X* **13**, 011005 (2023).
7. Moulton, P. Ti-doped sapphire: tunable solid-state laser. *Opt. News* **8**, 9 (1982).
8. Morgner, U. et al. Sub-two-cycle pulses from a Kerr-lens mode-locked Ti:sapphire laser. *Opt. Lett.* **24**, 411–413 (1999).
9. Prakash, R. et al. Two-photon optogenetic toolbox for fast inhibition, excitation and bistable modulation. *Nat. Methods* **9**, 1171–1179 (2012).
10. Xu, C. & Webb, W. W. Measurement of two-photon excitation cross sections of molecular fluorophores with data from 690 to 1050 nm. *J. Opt. Soc. Am. B* **13**, 481–491 (1996).
11. Leedle, K. J., Pease, R. F., Byer, R. L. & Harris, J. S. Laser acceleration and deflection of 96.3 keV electrons with a silicon dielectric structure. *Optica* **2**, 158–161 (2015).
12. Kfir, O. et al. Controlling free electrons with optical whispering-gallery modes. *Nature* **582**, 46–49 (2020).
13. Santori, C., Fattal, D., Vučković, J., Solomon, G. S. & Yamamoto, Y. Indistinguishable photons from a single-photon device. *Nature* **419**, 594–597 (2002).
14. Rugar, A. E. et al. Quantum photonic interface for tin-vacancy centers in diamond. *Phys. Rev. X* **11**, 031021 (2021).
15. Rizzo, A. et al. Massively scalable Kerr comb-driven silicon photonic link. *Nat. Photon.* **17**, 781–790 (2023).

16. Boes, A. et al. Lithium niobate photonics: unlocking the electromagnetic spectrum. *Science* **379**, eabj4396 (2023).
17. Riemensberger, J. et al. A photonic integrated continuous-travelling-wave parametric amplifier. *Nature* **612**, 56–61 (2022).
18. Xiang, C. et al. Laser soliton microcombs heterogeneously integrated on silicon. *Science* **373**, 99–103 (2021).
19. Xiang, C. et al. 3D integration enables ultralow-noise isolator-free lasers in silicon photonics. *Nature* **620**, 78–85 (2023).
20. Zhou, Z. et al. Prospects and applications of on-chip lasers. *eLight* **3**, 1–25 (2023).
21. Tran, M. A. et al. Extending the spectrum of fully integrated photonics to submicrometre wavelengths. *Nature* **610**, 54–60 (2022).
22. Corato-Zanarella, M. et al. Widely tunable and narrow-linewidth chip-scale lasers from near-ultraviolet to near-infrared wavelengths. *Nat. Photon.* **17**, 157–164 (2023).
23. Zhang, Z. et al. Photonic integration platform for rubidium sensors and beyond. *Optica* **10**, 752–753 (2023).
24. Ahmad, F. R., Tseng, Y. W., Kats, M. A. & Rana, F. Energy limits imposed by two-photon absorption for pulse amplification in high-power semiconductor optical amplifiers. *Opt. Lett.* **33**, 1041–1043 (2008).
25. Chang, L., Liu, S. & Bowers, J. E. Integrated optical frequency comb technologies. *Nat. Photon.* **16**, 95–108 (2022).
26. Liu, Y. et al. A photonic integrated circuit–based erbium-doped amplifier. *Science* **376**, 1309–1313 (2022).
27. Liu, Y. et al. A fully hybrid integrated erbium-based laser. Preprint at https://arxiv.org/abs/2305.03652 (2023).
28. Grivas, C., Shepherd, D. P., May-Smith, T. C., Eason, R. W. & Pollnau, M. Single-transverse-mode Ti:sapphire rib waveguide laser. *Opt. Express* **13**, 210–215 (2005).
29. Grivas, C. et al. Generation of multi-gigahertz trains of phase-coherent femtosecond laser pulses in Ti:sapphire waveguides. *Laser Photon. Rev.* **12**, 1800167 (2018).
30. Grivas, C., Corbari, C., Brambilla, G. & Lagoudakis, P. G. Tunable, continuous-wave Ti:sapphire channel waveguide lasers written by femtosecond and picosecond laser pulses. *Opt. Lett.* **37**, 4630–4632 (2012).
31. Yang, T.-T. et al. Widely tunable, 25-mW power, Ti:sapphire crystal-fiber laser. *IEEE Photon. Technol. Lett.* **31**, 1921–1924 (2019).
32. Wang, S.-C. et al. Laser-diode pumped glass-clad Ti:sapphire crystal fiber laser. *Opt. Lett.* **41**, 3217–3220 (2016).
33. Azeem, F. et al. Ultra-low threshold titanium-doped sapphire whispering-gallery laser. *Adv. Opt. Mater.* **10**, 2102137 (2022).
34. Wang, Y., Holguín-Lerma, J. A., Vezzoli, M., Guo, Y. & Tang, H. X. Photonic-circuit-integrated titanium:sapphire laser. *Nat. Photon.* **17**, 338–345 (2023).
35. Guo, Y. et al. Hybrid integrated external cavity laser with a 172-nm tuning range. *APL Photon.* **7**, 066101 (2022).
36. Guo, J. et al. E-band widely tunable, narrow linewidth heterogeneous laser on silicon. *APL Photon.* **8**, 046114 (2023).
37. Lukin, D. M. et al. 4H-silicon-carbide-on-insulator for integrated quantum and nonlinear photonics. *Nat. Photon.* **14**, 330–334 (2020).
38. Bouma, B. E. et al. Optical coherence tomography. *Nat. Rev. Methods Primers* **2**, 79 (2022).
39. Drexler, W. et al. *In vivo* ultrahigh-resolution optical coherence tomography. *Opt. Lett.* **24**, 1221–1223 (1999).
40. Ideguchi, T. et al. Coherent Raman spectro-imaging with laser frequency combs. *Nature* **502**, 355–358 (2013).
41. Major, A., Yoshino, F., Nikolakakos, I., Aitchison, J. S. & Smith, P. W. E. Dispersion of the nonlinear refractive index in sapphire. *Opt. Lett.* **29**, 602–604 (2004).
42. Shtyrkova, K. et al. Integrated CMOS-compatible Q-switched mode-locked lasers at 1900nm with an on-chip artificial saturable absorber. *Opt. Express* **27**, 3542–3556 (2019).
43. Byun, H. et al. Integrated low-jitter 400-MHz femtosecond waveguide laser. *IEEE Photon. Technol. Lett.* **21**, 763–765 (2009).
44. Franken, C. A. A. et al. Hybrid-integrated diode laser in the visible spectral range. *Opt. Lett.* **46**, 4904–4907 (2021).
45. Awschalom, D. D., Hanson, R., Wrachtrup, J. & Zhou, B. B. Quantum technologies with optically interfaced solid-state spins. *Nat. Photon.* **12**, 516–527 (2018).
46. Aslam, N. et al. Quantum sensors for biomedical applications. *Nat. Rev. Phys.* **5**, 157–169 (2023).
47. Bhaskar, M. K. et al. Experimental demonstration of memory-enhanced quantum communication. *Nature* **580**, 60–64 (2020).
48. Davis, E. J. et al. Probing many-body dynamics in a two-dimensional dipolar spin ensemble. *Nat. Phys.* **19**, 836–844 (2023).
49. Evans, R. E. et al. Photon-mediated interactions between quantum emitters in a diamond nanocavity. *Science* **362**, 662–665 (2018).
50. Lukin, D. M. et al. Multiemitter cavity quantum electrodynamics in 4H-silicon carbide-on-insulator photonics. In *CLEO 2023 Fundamental Science*, Technical Digest Series FTu3C.4 (Optica Publishing Group, 2023).
51. Catanzaro, D., Lukin, D. M., Lustig, E., Guidry, M. A. & Vučković, J. Cryogenic fiber-coupled waveguide probe co-integrated with electrical control lines. In *CLEO 2023 Science and Innovations*, Technical Digest Series JTu2A.47 (Optica Publishing Group, 2023).
52. Nagy, R. et al. Quantum properties of dichroic silicon vacancies in silicon carbide. *Phys. Rev. Appl.* **9**, 034022 (2018).
53. Levonian, D. et al. Optical entanglement of distinguishable quantum emitters. *Phys. Rev. Lett.* **128**, 213602 (2022).
54. Newman, Z. L. et al. Architecture for the photonic integration of an optical atomic clock. *Optica* **6**, 680–685 (2019).
55. Spencer, D. T. et al. An optical-frequency synthesizer using integrated photonics. *Nature* **557**, 81–85 (2018).
56. He, C. et al. Ultra-high Q alumina optical microresonators in the UV and blue bands. *Opt. Express* **31**, 33923–33929 (2023).
57. Li, M. et al. Integrated pockels laser. *Nat. Commun.* **13**, 5344 (2022).
58. Zhao, H. et al. Visible-to-near-infrared octave spanning supercontinuum generation in a silicon nitride waveguide. *Opt. Lett.* **40**, 2177–2180 (2015).
59. Ledezma, L. et al. Intense optical parametric amplification in dispersion-engineered nanophotonic lithium niobate waveguides. *Optica* **9**, 303–308 (2022).
60. Burton, H., Debardelaben, C., Amir, W. & Planchon, T. A. Temperature dependence of Ti:sapphire fluorescence spectra for the design of cryogenic cooled Ti:sapphire CPA laser. *Opt. Express* **25**, 6954–6962 (2017).
61. Soykal, Ö. O., Dev, P. & Economou, S. E. Silicon vacancy center in 4 *H*-SiC: Electronic structure and spin-photon interfaces. *Phys. Rev. B* **93**, 081207(R) (2016).

Methods

Device fabrication

Thin-film Ti:SaOI is produced by an adaptation of the grinding-and-polishing approach for silicon-carbide-on-insulator platform described in ref. 37. Several approaches and different crystal orientations are explored in this work: to produce the thin films used to demonstrate a microdisk laser, a c-plane (0001) Ti:sapphire wafer die (absorption coefficient at 532 nm $\alpha_{532} = 0.53\ cm^{-1}$, 5 mm × 5 mm) is bonded to an undoped sapphire wafer using an interfacial SiO_2 layer (thickness of 3 μm) deposited by plasma-enhanced chemical vapour deposition, which serves as the buried oxide layer. The stack is then processed in a wafer grinder (DAG810, Disco), followed by chemical–mechanical polishing (POLI-400L from G&P Technology) and thinning by reactive-ion etching in BCl_3 plasma (PlasmaTherm Versaline ICP) to the target thickness of 350 nm. The fabrication method does not constrain the thickness of the Ti:sapphire layer, which can be precisely controlled by the final dry etching step. For subsequent amplifier and waveguide demonstration, we use an a-plane (1120) Ti:sapphire wafer die ($\alpha_{532} = 6.2\ cm^{-1}$, 6 mm × 8 mm), bonded to undoped sapphire using the same process. The bonded Ti:sapphire dies are then ground and polished in a precision lapping system (PM5, Logitech), followed by the same reactive-ion etching process to reach a target thickness of 450 nm.

Microdisk resonators are fabricated by photolithography. Photoresist (S1822, Shipley) is spun on a Ti:SaOI film and patterned in a direct write lithography system (Microwriter ML3, Durham Magneto Optics). An optimized photoresist reflow process is then applied[50], and the pattern is transferred to the Ti:sapphire layer through a BCl_3 plasma reactive-ion etch that minimizes surface roughness. A surface roughness of 1.6 Å RMS is measured using atomic force microscopy. Afterwards, the underlying SiO_2 is undercut in hydrofluoric acid.

Amplifiers and waveguide lasers are fabricated using electron-beam lithography. A chromium hardmask (200 nm) is deposited on the Ti:SaOI film by electron-beam evaporation. Chromium is chosen to allow for the etching of sapphire with sufficient selectivity (4:1). Electron-beam photoresist (FOx-16, Corning) is spun afterwards and a 50-keV electron-beam lithography system (Voyager, Raith) is used to define the pattern. Limitations of the lithography system necessitated the confinement of devices to a 0.5 × 0.5 mm area to avoid stitching errors. The pattern is transferred into the chromium mask by a Cl_2 and O_2 plasma, and subsequently into sapphire by a BCl_3 etch. Subsequently, the chromium hard mask is stripped through wet etching using chromium etchant and Piranha solution. Devices are then capped with an initial layer of flowable oxide (FOx-16, Dow Corning), followed by an extra SiO_2 layer through high-density plasma chemical vapour deposition (PlasmaTherm), and were annealed at 800 °C in air. Facets for edge coupling of devices were created either through wafersaw dicing followed by focused-ion-beam milling or through laser stealth dicing (see Supplementary Fig. 1 for an illustration of fabrication process flow).

Device design

Waveguide spirals for the amplifiers are designed following ref. 62 to minimize mode mixing during propagation. The spiral waveguides have a thickness of 450 nm and a width of 1.5 μm. These dimensions were chosen to reduce scattering losses by the sidewalls, provide optimal confinement of both the pump and signal mode and allow for low-loss bends. Amplifiers with lengths of 3.4 mm, 8.1 mm and 0.485 mm are studied in this work. The shortest amplifier is a straight waveguide with a width of 900 nm, extending across the chip.

The waveguide lasers use a spiral waveguide amplifier with a length of 3.2 mm, a thickness of 450 nm and a width of 1.5 μm. A microring resonator with a diameter of 80 μm and width of 650 nm is used as the re-circulating element, and coupling gaps of 325 nm, 375 nm and 425 nm were studied. The width of the ring waveguide was chosen such that a single transverse electric mode is supported at a given wavelength. A platinum microheater is patterned on top of the microring resonator for thermo-optic wavelength tuning. Although not included in this work, a thermal phase-shifting element on the waveguide section would allow for an additional degree of freedom in the laser tuning control.

Quantum efficiency of waveguide gain medium

A reduction of the gain medium efficiency through introduction of non-radiative decay rates would be measured as a reduced excited-state lifetime. We characterize the Ti:SaOI waveguide fluorescence in the time domain by exciting with a weak modulated pump and by detecting emission rate using a superconducting nanowire single-photon detector, and we observe a purely single-exponential decay with a lifetime of 3.09 μs, consistent with the lifetimes reported in the literature for bulk Ti:sapphire[5].

Characterization of the waveguide amplifier

Light is coupled from free-space on-and-off chip using microscope objectives (M-plan NIR 100, Mitutoyo). The temperature of the sample substrate is maintained at 290 K throughout the experiments. The 532-nm pump source is a frequency-doubled diode-pumped solid-state laser (Verdi V10, Coherent) and is delivered onto the chip either from one or both facets of the waveguide or in the opposite direction to the signal. Unless otherwise stated, single-side pumping is used. For continuous-wave amplification experiments, a commercial Ti:sapphire laser (SolsTiS, M Squared) is used, which has a tuning range of 700–1,000 nm. Small-signal gain per unit length is measured for an input power of 0.10 mW. For characterization of small-signal gain in the 0.485-mm long waveguide (Fig. 2b) requiring a resolution of less than 0.1 dB, the pump and the signal are chopped and the amplification is extracted from the time-dependent signal recorded on a silicon photodetector. For small-signal gain characterization in 8-mm amplifiers, an optical spectrum analyser (Yokogawa AQ6370D) is used to obtain the output signal with and without the pump laser. This measurement does not take into account the passive waveguide losses. Wavelength-dependent passive waveguide loss is measured from the statistical analysis of waveguides of different lengths. Total passive transmission through the 8-mm amplifier, including insertion losses, is −14 dB. Cumulative off-chip amplification is represented by the difference between the measured on-chip amplification and passive loss at the given wavelength in Fig. 2c. The finite-difference time-domain simulations indicate back reflections from facets of less than 7%. To record the maximum amplified power output (Fig. 2d), the double-side pumped scheme is used. To infer the output power at the chip, the measured output power is corrected for objective losses (transmission of 0.85). For the pulsed-amplification experiment, a picosecond mode-locked Ti:sapphire laser (Tsunami, Spectra-Physics) is used. The $sech^2$ fit to the spectrum of the pulse shows a pulse duration of 2.2 ps, in agreement with the auto-correlator measurement. To measure the dependence of amplification and output pulse energy on the repetition rate, the intrinsic repetition rate of the laser (80 MHz) is reduced by an electro-optic modulator pulse picker (Conoptics) with a measured rejection ratio of 6.2×10^3.

Waveguide laser measurement

Laser characterization experiments use the same setup described in the waveguide amplifier section, with the addition of electrical microprobes to deliver power to the microheater. For precise and accurate measurement of the lasing wavelength, a wavemeter is used (WS7, HighFinesse). Using real-time wavelength reading, a feedback loop is implemented to tune and stabilize the laser within a mode-hop-free tuning range of the microheater (Fig. 3d). The heterodyne linewidth measurement was performed with a commercial Ti:sapphire laser (SolsTiS, M Squared). The photodetector signal was analysed with an

electrical spectrum analyser (Agilent PXA N9030A) with a resolution bandwidth of 100 kHz.

The demonstration of Ti:SaOI laser in diode-pumped operation was performed as follows. A single-mode green laser diode with a maximum output power of 110 mW was used (PLT5 5jo20B from OSRAM, in a TO-56-3 package). The laser diode was installed in a TE-Cooled Mount (LDM56, Thorlabs) and powered by a laser diode driver (LDC210C, Thorlabs). The laser diode output was collimated and coupled to the Ti:SaOI chip by free space. Single-mode lasing at two wavelengths of operation is demonstrated by tuning the microheater (Extended Data Fig. 1). The efficiency of pump coupling to chip was limited to about 16% but can be improved substantially with mode overlap engineering and efficient direct-contact coupling, as demonstrated previously for silicon-nitride photonics[22]. This approach can enable tunable Ti:SaOI chip-scale lasers in a butterfly package, as has been previously demonstrated in other platforms[63].

Data availability

The data used to support the findings in this work are presented in the main text and Supplementary Information.

62. Chen, T., Lee, H., Li, J. & Vahala, K. J. A general design algorithm for low optical loss adiabatic connections in waveguides. *Opt. Express* **20**, 22819–22829 (2012).
63. van Rees, A. et al. Long-term absolute frequency stabilization of a hybrid-integrated InP-Si_3N_4 diode laser. *IEEE Photon. J.* **15**, 1502408 (2023).

Acknowledgements We thank C. Langrock for his help with lapping and polishing, K. Yang for the discussions and guidance on fibre tapering, L. Mandyam for technical support in device fabrication and M. M. Fejer for access to laboratory equipment. We acknowledge funding support from the IET A. F. Harvey Prize, the Vannevar Bush Faculty Fellowship from the US Department of Defense, DARPA LUMOS and the AFOSR under award no. FA9550-23-1-0248. J.Y. acknowledges support from the National Defense Science and Engineering Graduate (NDSEG) Fellowship. K.V.G. acknowledges support from the Research Foundation—Flanders (12ZB520N). Part of this work was performed at the Stanford Nano Shared Facilities (SNSF)/Stanford Nanofabrication Facility (SNF), supported by the National Science Foundation under award no. ECCS-2026822.

Author contributions J.Y. and K.V.G. designed the devices. J.Y., K.V.G., D.M.L. and G.H.A. fabricated the devices. J.Y., K.V.G., D.M.L., M.A.G. and A.D.W. ran the device simulations. J.Y., K.V.G., D.M.L., M.A.G. and A.D.W. assisted with the experimental setup. J.Y., K.V.G., D.M.L. and M.A.G. conducted the measurements on the microdisk lasers. J.Y., K.V.G., D.M.L. and M.A.G. conducted the measurements on the waveguide amplifiers. J.Y., K.V.G. and D.M.L. conducted the measurements on the waveguide lasers. J.Y. and D.M.L. conducted the cavity QED experiment. J.Y., K.V.G. and D.M.L. analysed the data. All authors helped with editing the Article. J.V. supervised the work.

Competing interests J.Y. and D.M.L. are cofounders of Brightlight Photonics, which is commercializing integrated Ti:sapphire lasers. K.V.G. is an advisor to Brightlight Photonics. J.Y., K.V.G. and D.M.L. hold equity in Brightlight Photonics. J.V., D.M.L., M.A.G. and G.H.A. are coinventors on a patent application related to integrated Ti:sapphire lasers (patent no. WO 2021/022188). J.V., J.Y., K.V.G. and D.M.L. are coinventors on a patent application related to integrated Ti:sapphire amplifiers.

Additional information

Supplementary information The online version contains supplementary material available at https://doi.org/10.1038/s41586-024-07457-2.

Correspondence and requests for materials should be addressed to Jelena Vučković.

Peer review information *Nature* thanks Emir Salih Mağden, Johann Riemensberger and the other, anonymous, reviewer(s) for their contribution to the peer review of this work.

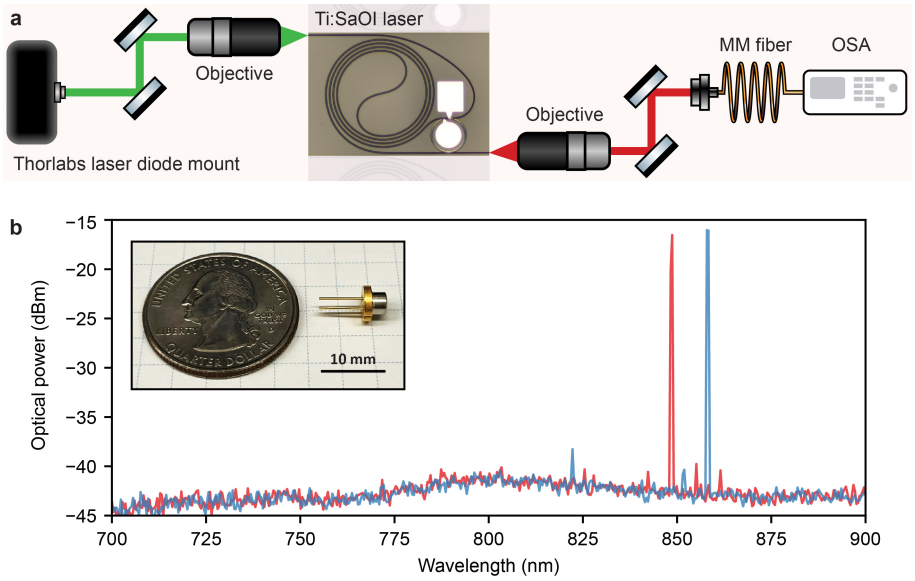

Extended Data Fig. 1 | Diode-pumped on-chip Ti:Sapphire laser. (a) Diagram of the measurement setup used in the diode-pumping experiments (MM: multi-mode, OSA: optical spectrum analyzer). (b) Measured optical spectrum of single-mode lasing at 848.7 nm and 858.3 nm, with a SMSR of 23.2 dB and 22.2 dB, respectively. (Inset) Image of the diode package used in these experiments.